phys. stat. sol. (b) **198**, 5 (1996)

Subject classification: 63.20 and 78.20; 62.50; 71.70; S5; S7; S8; S9

Max-Planck-Institut für Festkörperforschung, Stuttgart[1])

Semiconductors under Uniaxial Strain

By

M. CARDONA

(Received August 12, 1996)

Uniaxial strain, having a larger number of irreducible components, yields in principle more information than its hydrostatic counterpart. It has, however, the drawback that its magnitude is limited by sample fracture. We discuss the methods of application of uniaxial stress to solid samples for the purpose of performing spectroscopic measurements. We then present some of the highlights of such measurements, concerning phonons and electronic states in semiconductors.

1. Introduction

The strain tensor $\hat{e}$, being symmetric, has in general six independent components. Its trace determines the hydrostatic component of the strain ($e_H = \mathrm{tr}\,\hat{e}/3$). When $e_H \cdot \mathbf{1}$ ($\mathbf{1}$ is the unit matrix) is subtracted from $\hat{e}$, a traceless tensor with five independent components is obtained which represents the most general traceless strain (sometimes called a "pure shear"). The tensor $e_H \cdot \mathbf{1}$, being invariant under all point group operations, leads to effects which exhibit the full space group symmetry of the crystal (changes of the lattice parameters can be taken care of by means of the Pikus and Bir transformation [1]). Hence the hydrostatic strain is said to belong to the irreducible representations A or Γ_1 of the space group (A_g or Γ_1^+ if the system is centrosymmetric). A similar symmetry analysis can be made for the five components of the traceless strain. In the cases of cubic symmetry the off-diagonal components of $\hat{e}$ transform according to a three-dimensional irreducible representation which is labeled $\Gamma_{25'}$ or T_{2g} for the diamond structure (Γ_4, Γ_{15} or T_2 for zincblende) while the remaining two independent components $1/\sqrt{2}\ (e_{yy} - e_{zz})$ and $1/\sqrt{6}\ (2e_{xx} - e_{yy} - e_{zz})$ belong to $\Gamma_{12}(E_g)$ in diamond and Γ_{12}, Γ_3 or E in zincblende. Hence, in the crystals with diamond and zincblende structure a general strain has three irreducible components which lead to three independent sets of spectra (one hydrostatic and two pure shear). The T_2 shear corresponds to a uniaxial deformation along the [111] direction while its E counterpart corresponds to a uniaxial deformation along [100]. The shear components are

$$\mathrm{E}: \quad \frac{e}{\sqrt{2}} \begin{pmatrix} 0 & & \\ & +1 & \\ & & -1 \end{pmatrix}, \qquad \frac{e}{\sqrt{6}} \begin{pmatrix} 2 & & \\ & -1 & \\ & & -1 \end{pmatrix};$$

[1]) Heisenbergstr. 1, D-70569 Stuttgart, Federal Republic of Germany.
e-mail: cardona@cardix.mpi-stuttgart.mpg.de

$$T_2: \quad e\begin{pmatrix}0&0&0\\0&0&1\\0&1&0\end{pmatrix}, \quad e\begin{pmatrix}0&0&1\\0&0&0\\1&0&0\end{pmatrix}, \quad e\begin{pmatrix}0&1&0\\1&0&0\\0&0&0\end{pmatrix}. \tag{1}$$

For simplicity we shall use here and in what follows the zincblende notation A_1, E, T_2 for both diamond and zincblende.

The magnitude of the hydrostatic strain that can be applied to a crystal is limited by the experimental equipment available and has received a big boost with the development of the diamond anvil cell (DAC). The sample is usually embedded in a fluid medium which transmits to it a hydrostatic *stress*. Only in cubic materials a hydrostatic *stress* corresponds to a hydrostatic *strain*. Moreover, most standard pressure transmitting fluids become viscous, glassy or even crystallize under the action of stress: The stress applied to the sample becomes then nonhydrostatic, its shear components being usually irreproducible. This problem is avoided, at least up to stresses of the order of 100 GPa, by using helium as pressure transmitting fluid. Within this range phase transitions occur. They may be irreversible and lead to destruction of the sample. Except for this fact, samples are usually found to be intact after releasing the hydrostatic stress.

When a uniaxial stress is applied to a sample with equipment such as that of Fig. 1 [2] (stress X along only one direction, all other components of the stress tensor $\hat{\sigma}$ equal to zero) only a relatively low stress (yield stress) can be reached before the sample breaks. The yield stress is usually not a material property but is determined by surface conditions, defects, details of the equipment, etc. It reaches typical values of 3 GPa for Si, 1.5 GPa for Ge, and 1 GPa for GaAs. Within this range, and contrary to the case of the much higher hydrostatic stresses reached in the DAC, most (but not all) effects

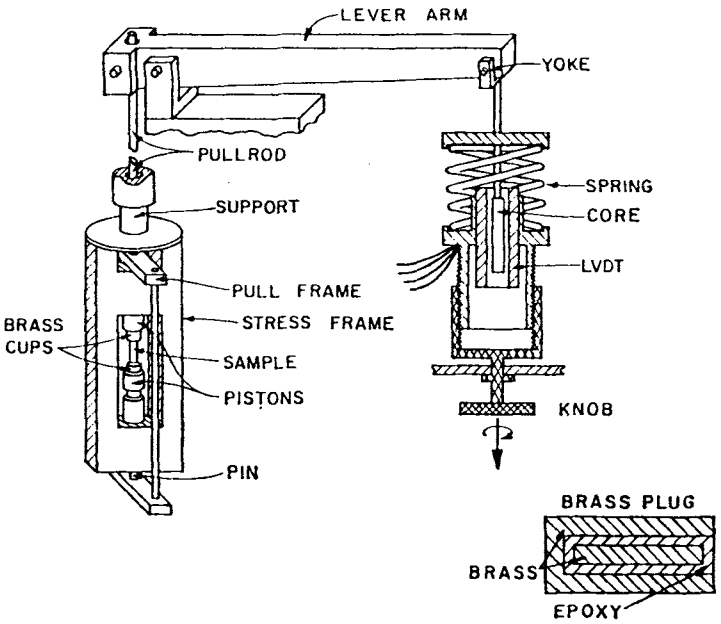

Fig. 1. Rig used for optical measurements under uniaxial stress. The applied force is measured by measuring the elongation of the spring with a linear variable differential transformer (LVDT) [2]

observed are linear in the stress (or strain). Nevertheless the stress, if kept below the yield value, often breaks the crystal symmetry without breaking the sample. For the zincblende structure, e.g., a [100] stress lowers the T_d cubic symmetry to the tetragonal D_{2d} while a [111] stress lowers it to the trigonal C_{3v}. Thus, degenerate states split and transitions forbidden to a given type of spectroscopy may become allowed.

In this paper we discuss the highlights of the effects of uniaxial stresses along [100] and [111] on the phonons and electronic states of crystals with diamond and zincblende structure. From these data the effects of the three irreducible components of the strain can be extracted. They suffice to calculate linear (sometimes even quadratic) effects of strain along any arbitrary direction.

2. Methods to Apply Uniaxial Stress

Maybe the most commonly used, time tested method to apply uniaxial stress to solids for optical and electronical experiments is that of Cuevas and Fritzsche (see Fig. 1) [2]. The stress is applied with a spring which acts on the sample via a 10/1 lever arm (to increase the force). One of the softest spots in the procedure is the point at which the force is applied to the sample (which has a typical cross section of $\approx 2\,\mathrm{mm}^2$). If this application is not uniform, early fracture results at points subjected to higher than average strains. A time-tested procedure to minimize this problem consists of glueing the sample with epoxy resin to a pair of brass cups into which holes, which snuggly accommodate the sample ends, have been drilled. These cups are mounted into a frame as

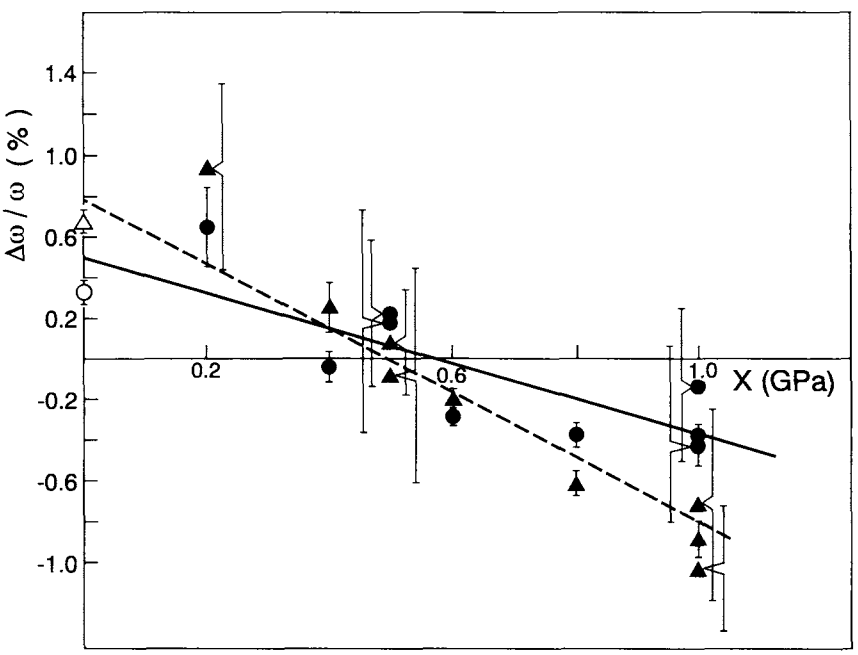

Fig. 2. Frequency shifts of the TA phonons of silicon upon application of a 1 GPa stress along [100]. The **k** directions are [100] (singlet) (– – –, ▲) and [010] (doublet) (———, ●). The points at $X = 0$ are ultrasonic velocity measurements; from [5]

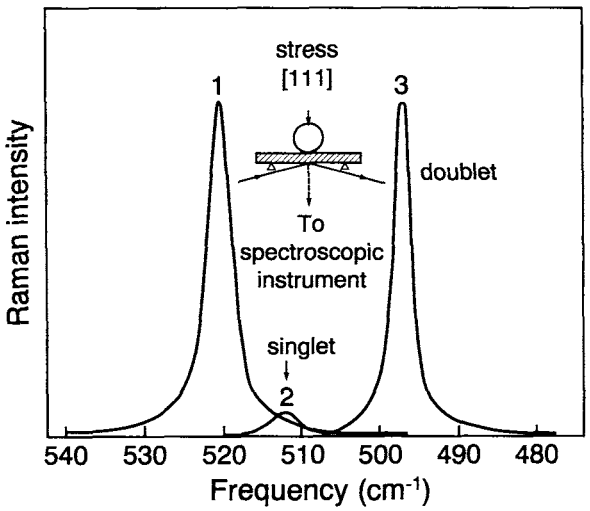

Fig. 3. Effect of a planar stress of 5 GPa, applied with the schematically drawn bending rig on a [111] silicon wafer, on the Raman phonons of silicon. The unstressed spectrum is labeled 1. The singlet and doublet, split by the stress, are labeled accordingly [8]

shown in Fig. 1. The force is applied to the lower cup through a pin mounted in a counterframe connected to the lever arm by means of a pullrod.

Alignment of all parts mentioned with respect to the sample axis is very important. The pressure is measured by either measuring the (calibrated) elongation of the spring [2] or by means of a stress gauge placed at a convenient spot along the system [3]. A long pullrod allows the fitting of the sample frame into a cryostat for work at low temperatures. The force generating spring can be replaced by other devices such as a pneumatic or hydraulic cylinder-piston system [4]. Stresses as high as 3 GPa can be reached (with Si samples).

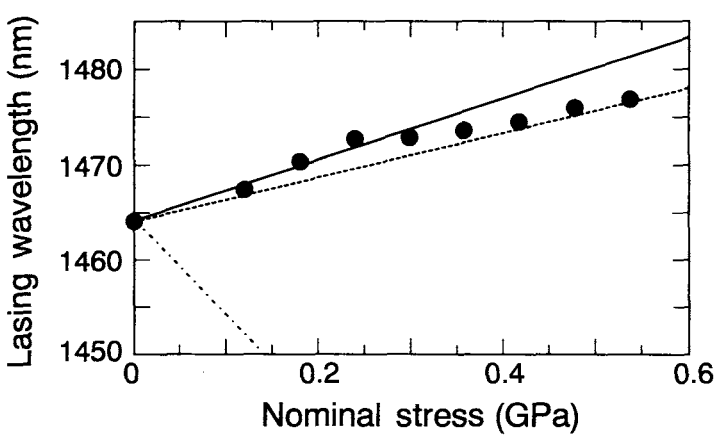

Fig. 4. The points indicate the measured variation of the lasing wavelength of a GaAs laser subjected to a uniaxial stress in a DAC. The solid line represents the variation expected if complete slippage with respect to the diamond faces takes place while the dash-dotted line represents the expectations for complete adhesion to the diamonds [9]. The dashed line shows the variation with a little friction present at the laser surfaces

The effects observed are *usually* linear in the strain components. In this case a given effect depends, in cubic materials, on three independent parameters (see (1)) which can be determined through measurements for stresses along [100] and [111] (plus sometimes hydrostatic pressure data). Redundant results are sometimes obtained, as a check, for stresses along [110]. Actually, a single parallelepiped with the stress direction along [110] and the side faces perpendicular to $[1\bar{1}0]$ and [001] often suffices to obtain all the information required.

A modified version of the frame of Fig. 1 has been used [5] to investigate the dependence of the phonon dispersion relations on uniaxial stress by means of inelastic neutron scattering. Fig. 2 shows the frequency shifts measured for the TA phonons of Si for **k** along the [100] and [010] directions and an applied stress of 1 GPa along [100]. Data are given for phonon polarizations parallel and perpendicular to the stress. The difference of the two slopes represents the effect of the pure shear stress while their weighted average (**k** ∥ [100] weight 1, **k** ∥ [010] weight 2) represents the effect of the hydrostatic stress component, which in this case is dominant. Note that the latter corresponds to a negative mode Grüneisen parameter $\gamma = -(\mathrm{d} \ln \omega / \mathrm{d} \ln V) = -1.7 \pm 0.2$ from $k = 2\pi/a$, in agreement with experiments at the X-point [6] and with *ab initio* calculations based on the electronic band structure [7].

The largest stresses have been reached by bending silicon slabs (30 mm diameter, 0.2 mm thick). We show in Fig. 3 a schematic of the rig used by Baptizmanskii et al. [8] for planar stress applied to a [111] Si wafer (isotropic planar stress is obtained when a

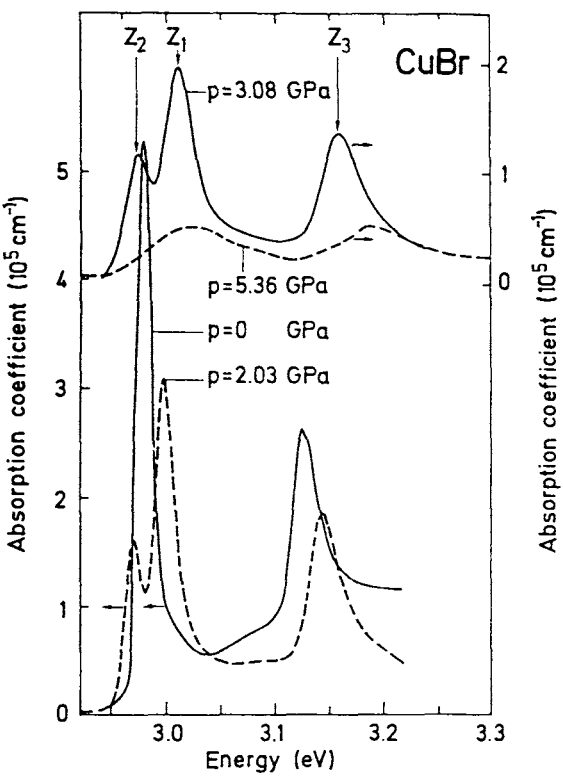

Fig. 5. Typical absorption spectra of a thin film of CuBr at 0, 2.03, 3.08, and 5.36 GPa at $T \approx 200$ K. The film was deposited on one of the anvils of a DAC. The frozen pressure transmitting fluid generated a uniaxial stress in the film. The data at 2.03 and 3.08 GPa show clearly the splitting of the exciton Z_{12} into Z_1 and Z_2 due to the uniaxial component of the stress [10]

force is applied at the center of the wafer). This figure also displays the Raman spectra of the $\mathbf{k} = 0$ optical phonons for zero stress and for a tensile planar stress corresponding to 5 GPa. Notice that the phonon peak splits by about 15 cm^{-1} while the main component (corresponding to a vibration perpendicular to [111]) down shifts by $\approx$22 cm^{-1}.

The DAC has also been used to apply uniaxial stresses, in particular to investigate the effect of such stresses on semiconductor lasers (frequency and threshold currents) [9]. Stresses of about 0.6 GPa have been reached by letting the diamonds bear directly on a parallelepiped sample. An interesting question is whether the in-plane strain is the same in the diamond faces which bear on the sample and in the corresponding sample faces (100% friction) or whether the sample glides with respect to the diamonds (no friction). This question is answered in Fig. 4: the laser wavelength of a GaAs laser shifts by an amount very close to the estimate for the no-friction, gliding case.

Another example of uniaxial stress applied with a DAC is seen in Fig. 5 [10]. In this case the DAC is operated with a standard gasket and alcohol as pressure transmitting fluid. The sample, in this case CuBr, is deposited as a thin film on one of the diamond faces and is in contact with the alcohol. The measurements are performed below 200 K: the alcohol freezes into a plastically deformable glass. Upon applying pressure, the frozen alcohol acts as a piston on the CuBr film and exerts a uniaxial stress which manifests itself by the splitting of the lowest edge exciton (Z_1–Z_2). The splitting increases linearly up to an applied stress of 3.5 GPa at which the film begins to deform plastically and the splitting decreases.

Another method to apply uniaxial stresses to thin films deposited pseudomorphically (i.e. with the same lateral lattice constant) on a substrate of similar structure has been used by the Missouri-Purdue group [11, 12]. A sample, consisting of film plus substrate,

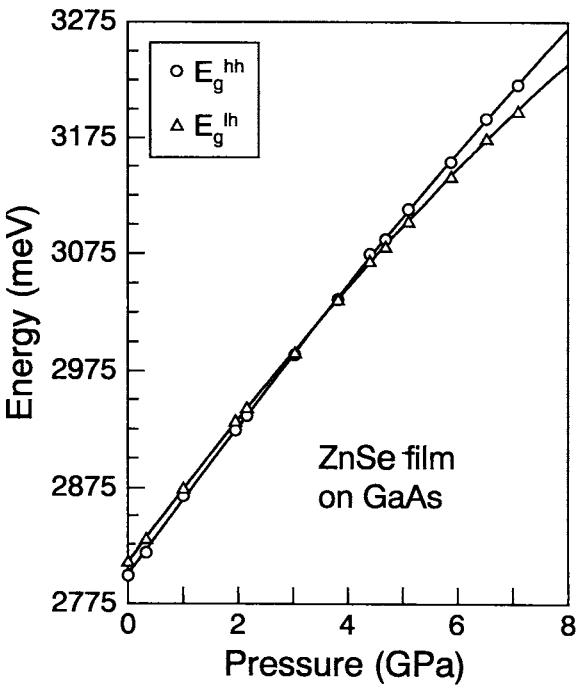

Fig. 6. Heavy and light hole exciton energies vs. pressure (in a DAC) of a ZnSe film on a GaAs substrate [11]

is placed in the conventional way in the DAC and the stress is applied hydrostatically to this composite sample (using argon as pressure transmitting fluid). While the thicker substrate is compressed hydrostatically, the difference in compressibilities (or bulk moduli) between substrate and sample film generates a uniaxial component of the strain in the latter. The film thus experiences a large hydrostatic and a smaller uniaxial strain as evidenced in Fig. 6 for a ZnSe film grown on GaAs. This figure shows the observed positions of the light hole (E_g^{lh}) and heavy hole (E_g^{hh}) excitons of ZnSe versus applied pressure. The large blue shifts are due to the hydrostatic component of the strain: This average corresponds rather closely to the shift found for a bulk ZnSe sample. A hh–lh splitting is seen, however, even at zero pressure. It is due to the differential in-plane compression induced by the fact that the lattice constant of ZnSe is larger than that of the GaAs substrate. The compressibility of ZnSe is also larger than that of GaAs and therefore the lattice constants of both materials become equal for an applied pressure of about 3.5 GPa: at this point the hh–lh vanishes; at higher pressures it even reverses sign (Fig. 6). In this manner in [11] the deformation potential b, which represents the hh–lh splitting under a shear strain, was determined to be $b = -1.14$ eV. It was also shown that the magnitude of b increases significantly with increasing hydrostatic pressure, a fact which reflects similar trends among the zincblende semiconductors versus lattice constant at zero pressure. This technique has also been used to obtain information about phonon deformation potentials [13, 14].

3. Internal Stress Parameters

For crystals with more than one atom per primitive cell (PC), the lattice parameters often do not suffice to determine the details of the atoms in the PC [15]. Likewise, the elastic constants do not suffice to determine the atomic displacements linear in stress: so-called internal strain parameters are needed.

Little quantitative information is available for the internal strain parameters which relate to applied uniaxial stresses. We discuss here the case of diamond- and zincblende-type materials with two atoms per unit cell. No internal strain parameter is needed for a uniaxial stress applied along [100] since the atomic planes perpendicular to this direction remain equidistant after the application of stress. For a [111] stress, however, an internal strain parameter is needed, for diamond as well as for zincblende, in order to specify the relative position of the two atoms in the unit cell. Note that two extreme cases are possible: either the bond length along [111] remains constant upon application of the traceless stress (rigid bond length) or it deforms like the macroscopic crystal (affine deformation). The intermediate situation which usually obtains is represented by Kleinman's internal strain parameter ζ: $\zeta = 1$ corresponds to a rigid bond length while $\zeta = 0$ corresponds to the affine deformation of the crystal. Note that a change in bond length, i.e., of the separation between the two sublattices without macroscopic deformation, is equivalent to the displacement pattern of an optical phonon at $\mathbf{k} = 0$. A stress will induce such displacement if and only if the stress has a component of the same symmetry as such an optical phonon [15]. In the zincblende structure (similar reasoning applies to diamond) the phonon has Γ_{15} symmetry. Hence a [100] stress (Γ_{12} symmetry) does not call for an internal strain parameter while a [111] stress, of Γ_{15} symmetry, does.

The information available on ζ is not very precise. Experimental data are available only for germanium, silicon [16], diamond, and GaAs [17] while semiempirical [18 to 20]

and *ab initio* [21] calculations are available for a wide range of materials of the family. In the latter, the total energy (electrons + ions) is computed, using band structure techniques, for the crystal under a [111] stress with the bond length as parameter. The bond length, and thus ζ, is then determined by minimizing the total energy. The experimental determination is based on the observation, by X-rays scattering, of the increase in intensity with stress of a forbidden or nearly forbidden reflection.

The few available experimental and theoretical data reveal the following trend:

1. Materials corresponding to the first row of the periodic table (diamond, BN) have $\zeta \approx 0.1$, i.e., they deform in an affine manner.

2. Materials only with atoms not belonging to the first row have $\zeta \approx 0.5$, i.e., the bond length shows considerable rigidity upon application of a [111] stress.

3. Materials with only one atom belonging to the first row show intermediate behavior (e.g., BP, $\zeta \approx 0.3$ [21]).

These trends can be easily understood by expressing ζ as a function of Keating's valence force field parameters α (bond stretching) and β (bond bending) [18],

$$\zeta = \frac{\alpha - \beta}{\alpha + \beta} . \tag{2}$$

The small values of ζ for diamond-row materials reflect the fact that $\alpha \approx \beta$, i.e., that the resistance to bond bending is as large as that to bond stretching. For other materials $\zeta \approx 0.5$, i.e., $\beta \approx 0.3\alpha$. In this case bond bending is much easier than bond stretching. The case $\alpha \approx \beta$ reflects the strong *covalency* of the bond in diamond (and BN). $\beta = 0.3\alpha$ reflects a loss of covalency which is not related to increasing *ionicity* but to increasing *metallicity*. The structural description of semiconductor nanostructures (e.g., MQWs) requires a large number of unit cell parameters which become, upon application of stress, internal strain parameters. Very little information is available about them, a fact which hinders theoretical work on both electronic and vibronic properties.

4. Phonons under Uniaxial Stresses

4.1 The diamond structure

We have already shown in Fig. 2 and 3 examples of effects of stress on phonons. Most of the available information has been obtained by Raman spectroscopy (phonons at Γ) with stressing rigs similar to that in Fig. 1. Let us first discuss the diamond structure case. The hydrostatic component of the stress shifts the frequency ω_R of the Γ-phonons without splitting them. This shift is represented by the mode Grüneisen parameter γ_R:

$$\gamma_R = -\frac{\mathrm{d} \ln \omega_R}{\mathrm{d} \ln V} , \tag{3}$$

where V is the sample volume. Either of the two irreducible shear components of (1) produces splittings into a singlet and a doublet. These splittings are observed by applying a stress along either [100] or [111] with the rig of Fig. 1. We show the corresponding experimental frequencies versus applied stress for Si [20] and diamond [22] in Fig. 7. The singlet and doublet can be identified by means of polarization selection rules. Let us consider, as an example, the case of a [100] stress of magnitude X. The stress tensor can be decomposed into a hydrostatic and a pure shear (traceless) component,

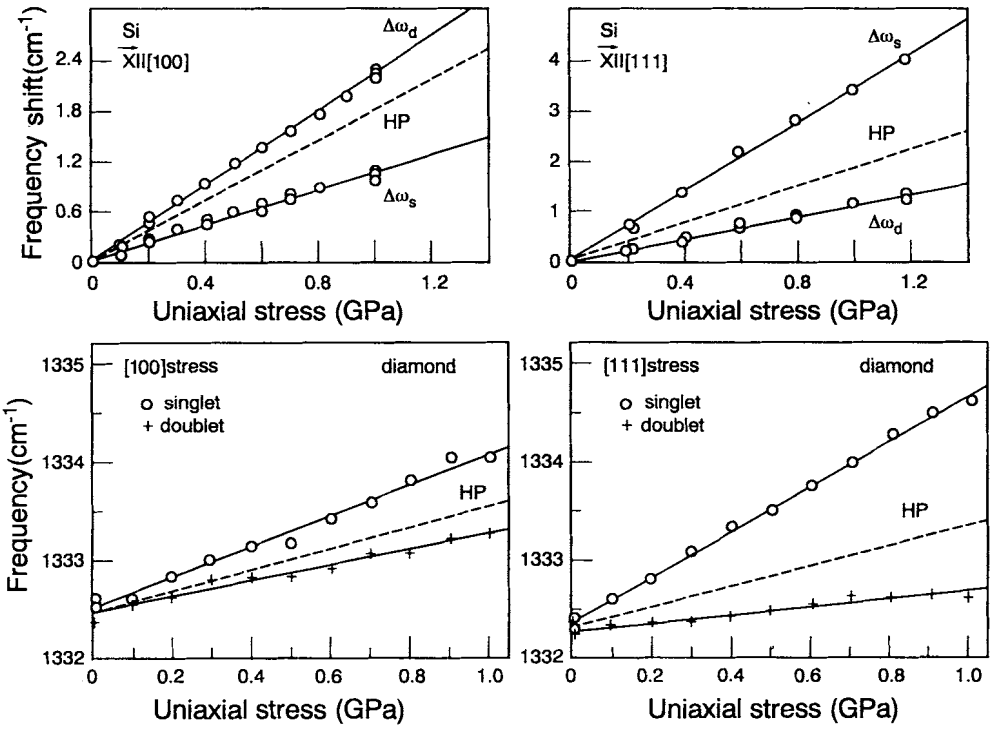

Fig. 7. Shifts and splittings experienced by the Raman phonons of diamond [22] and silicon [20] under the action of a uniaxial stress along the [100] and [111] directions. The dashed lines indicate the shift induced by the hydrostatic component of the stress. Note that the sign (singlet–doublet) of the splitting for [100] stress in silicon is opposite to all other cases displayed (see text)

$$X\begin{pmatrix}1 & & \\ & 0 & \\ & & 0\end{pmatrix} = -\frac{X}{3}\begin{pmatrix}1 & & \\ & 1 & \\ & & 1\end{pmatrix} + \frac{X}{3}\begin{pmatrix}2 & & \\ & -1 & \\ & & -1\end{pmatrix}. \tag{4}$$

The effect of the hydrostatic stress is related to γ_R by

$$\Delta\omega_R^h = -\omega_R\gamma_R(S_{11} + 2S_{12})\,X\,. \tag{5}$$

It corresponds in Fig. 7 to the weighted average ($1\times$singlet, $2\times$doublet) of the shifts of Fig. 7. The effects of [100] and [111] shear are represented by the dimensionless deformation potentials $\tilde{K}_{11} - \tilde{K}_{12}$ and $\tilde{K}_{44}$, respectively (sometimes $(p_{11} - p_{12})/\omega_0^2$ and p_{44}/ω_0^2 are used instead of $\tilde{K}_{11} - \tilde{K}_{12}$ and $\tilde{K}_{44}$, respectively). The singlet–doublet splittings are then given by

$$\begin{aligned}\Delta_{s,d}^{100}\omega_R &= \frac{\tilde{K}_{11} - \tilde{K}_{12}}{2}\,\omega_R X\,,\\ \Delta_{s,d}^{111}\omega_R &= \frac{\tilde{K}_{44}}{2}\,\omega_R X\,.\end{aligned} \tag{6}$$

Table 1
Measured dimensionless deformation potentials of the Raman phonons of diamond and silicon [22]. Results of ab initio calculations are given in parentheses. Note the sign reversal of $\tilde{K}_{11} - \tilde{K}_{12}$ discussed in the text

	diamond		silicon	
$\tilde{K}_{11} - \tilde{K}_{12}$	−1.04	(−1.38) [23]	+0.46	(0.26 [23], 0.46 [24])
$\tilde{K}_{44}$	−1.9	(−2.1) [23]	−0.70	(−0.6 [23], −0.9 [24])
γ_R	1.06	(0.95) [23]	0.98	(0.9 [23], 0.99 [24])

The diamond data of Fig. 7, obtained under a compressive stress X, show that for both stress directions the singlet component shifts up in frequency, even after the hydrostatic part is subtracted. This can be naively interpreted as due to the fact that the singlet vibrates along the direction of a compression (the doublet, however, along an expansion) and therefore the corresponding force constant should become stiffer. The data for silicon, however, while supporting this argument for $\mathbf{X} \parallel [111]$, are qualitatively different for $\mathbf{X} \parallel [100]$: the singlet *decreases* under compression. The answer to this paradox is found by considering that the pure shear component of (4) does not alter the bond length (for a [111] stress it does and the argument given above follows). The [100] *compressive* shear does not change the bond lengths. It simply bends the bonds away from the [100] axis. If we assume the bond stretching forces to be dominant, they effectively decrease for the singlet mode since they must be projected on the [100] axis (this introduces a factor of $\cos^2 \varphi$ where φ is the angle between the bond and [100]; φ increases when compressing along [100]). We have therefore rationalized the results of Fig. 7 for silicon. Now the surprising fact is that for a [100] compressive stress applied to diamond the singlet increases in frequency. This can also be understood if we recall that bond bending forces are very important in diamond (they were neglected in the argument given above for Si). They contribute a restoring force which, for the singlet, increases upon compression (due to anharmonicity) more than the geometric, $\cos^2 \varphi$ effect discussed above, and lead to an increase in frequency [20].

Detailed *ab initio* calculations support the argument given above as can be seen in Table 1. In this table we compare experimental values of γ_R, $\tilde{K}_{11} - \tilde{K}_{12}$, and $\tilde{K}_{44}$ for diamond and silicon with those obtained in ab initio calculations based on either pseudopotential [23] or LMTO [24] band structures.

Recent *ab initio* calculations of the shear splittings of the Raman phonon of BN yield the same signs for $\tilde{K}_{11} - \tilde{K}_{12}$ and $\tilde{K}_{44}$ as in diamond [25]. This is not surprising in view of the strong covalent character of BN which is also reflected in the value of ζ (= 0.12) [21].

4.2 The zincblende structure

For the diamond structure, discussed in Section 4.1, the optical phonons at Γ are even under inversion and therefore Raman but not ir-active. In zincblende there is no inversion symmetry. The Γ phonons are thus both Raman and ir-active. For the large wavevector transfers $\mathbf{k}$ invoked in Raman scattering they split into longitudinal (i.e., vibrating along $\mathbf{k}$) and transverse (i.e., vibrating perpendicular to $\mathbf{k}$). The splitting is related

to the transverse effective charge e_T^* through

$$\omega_{LO}^2 - \omega_{TO}^2 = \frac{4\pi(e_T^*)^2}{\mu V_c \varepsilon_\infty}, \tag{7}$$

where μ is the reduced mass of the two atoms, V_c the unit cell volume, and ε_∞ the ir dielectric constant. The LO–TO splitting introduces a new quantization axis along **k**. Since $\omega_{LO} - \omega_{TO}$ is much larger than the splitting induced by the stress, the primary quantization axis is determined by **k** and not by the stress (contrary to the diamond structure). Depending on the direction of **k** with respect to the stress axis, the LO phonons are singlet- (vibration parallel to the stress) or doublet-like (perpendicular to the stress). For backscattering in the rig of Fig. 1 only the doublet-like LO phonon can be observed. For the TO phonon, however, it is possible to see singlet and doublet components. In order to obtain all independent stress-induced shifts, Raman measurements with a laser line below the absorption edge of GaAs were performed in [26]. This allows measurements in forward and 90° scattering configurations since the sample is transparent to the laser light. For near-forward scattering one can have a **k**-vector parallel to the stress direction and thus observe the singlet LO.

A complete set of data obtained for stresses along [100] and [111] is shown in Fig. 8. It becomes clear in this figure that the L–T splitting of the singlet decreases upon application of the stress which, according to (7), implies that the compressive stress lowers the effective charge. (V_c and ε_∞ are also affected by the stress as represented by the com-

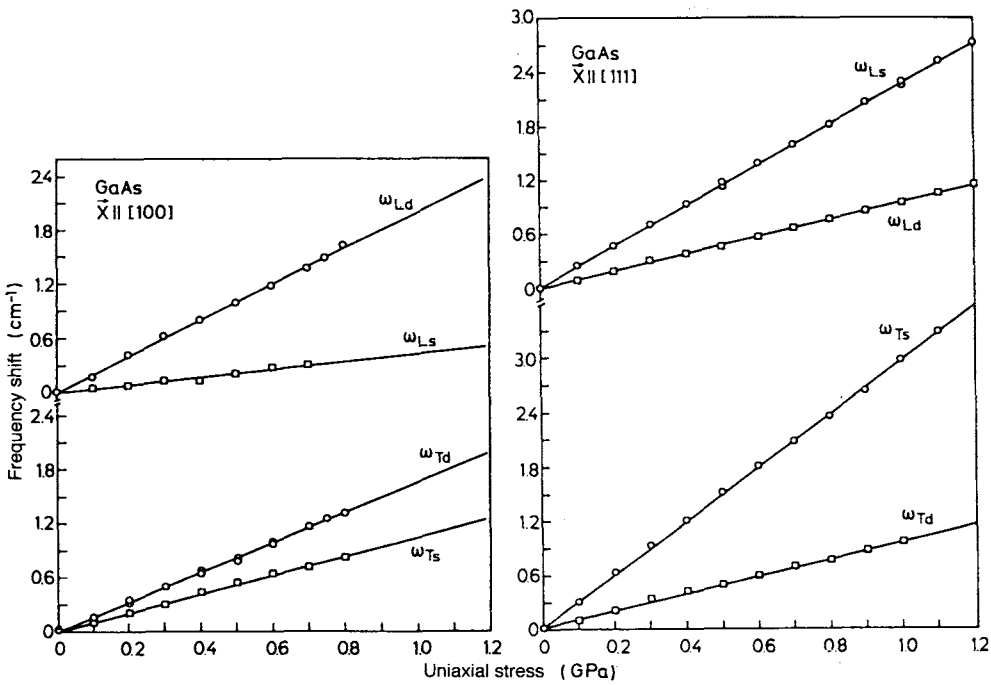

Fig. 8. Splittings and shifts of the LO and TO phonons of GaAs under the action of uniaxial stress along [100] and [111] [26]

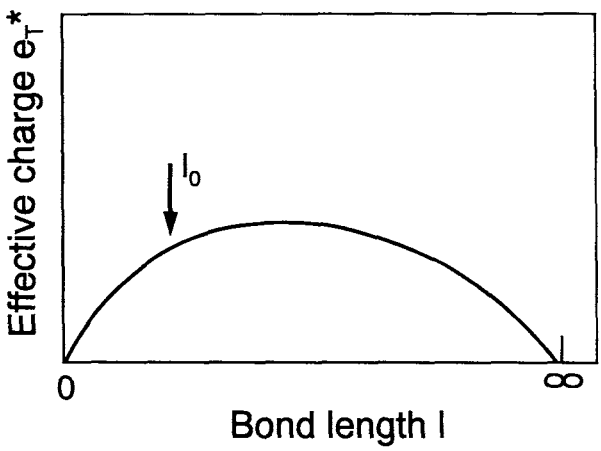

Fig. 9. The dependence of the transverse effective charge e_T^* of a zincblende-type bond on bond length l (the so-called Laffer curve[2])). The arrow labeled l_0 represents the equilibrium bond length at zero pressure

pressibility and the elastooptic constant. However, these effects are smaller than the changes in e_T^*.)

The changes in e_T^* induced by the strain tensor can be represented by a fourth rank tensor (note that e_T^* is actually a second rank tensor which connects a vector, the phonon displacement, with another vector, the induced dipole moment). It can, like in the case of $\tilde{K}$, be represented by three independent components which are called [26] M_{11}, M_{12}, and M_{44}: $M_{11} + 2M_{12}$ represent the hydrostatic effect, $M_{11} - M_{12}$ the effect of [100] shear, and M_{44} the effect of [111] shear. Ample evidence suggests that $M_{11} + 2M_{12}$ is positive, i.e., that compressive hydrostatic pressure decreases e_T^* in all zincblende-like semiconductors except SiC [26 to 28].

A qualitative insight in the behavior of e_T^* just described can be obtained from the curve in Fig. 9 which describes the simplest possible dependence of e_T^* versus bond length l (the so-called Laffer curve[2])). For $l = 0$ $e_T^* = 0$ since no charge separation occurs. For $l = \infty$ also $e_T^* = 0$ since the component atoms are neutral. The dynamical charge e_T^* has a maximum somewhere between $l = 0$ and ∞. Whether e_T^* increases with decreasing l (i.e., with increasing compressive pressure) depends on whether the equilibrium $l = l_0$ lies to the right or the left of the maximum in e_T^*. The decrease in e_T^* when compressing, found experimentally (exception: SiC), implies that it lies to the left.

Semiempirical values of $M_{11} - M_{12}$ and M_{44} can be obtained from the derivative of e_T^* versus bond length and the geometrical changes in the bonds introduced by the strain.

Table 2

Tensor coefficients which describe the effect of hydrostatic ($M_{11} + 2M_{12}$) and shear strain [$(M_{11} - M_{12}), M_{44}$] on the ir effective charge e_T^* of GaAs

	$M_{11} + 2M_{12}$	$M_{11} - M_{12}$	M_{44}
experiment	3.9 ± 1	1.6 ± 0.2	1.1 ± 0.2
calculation	1.9	1.5	0.9

[2]) Named after the American economist A. B. Laffer who applied a similar curve to interpret the behavior of the state revenue versus tax rate.

Table 2 shows the values of $M_{11} + 2M_{12}$, $M_{11} - M_{12}$, and M_{44} measured for GaAs, together with semiempirical calculations which use de_T^*/dl as the only adjustable parameter. Estimates for many zincblende-type semiconductors can be found in [28]. No *ab initio* calculations of the dependence of e_T^* on strain are yet available.

5. Electron Energy Bands versus Uniaxial Strain

The effect of strain on electronic states has been the object of considerable attention since the mid 1950's [1].The original motivation was the estimation of electron–phonon interaction in order to interpret the measured conductivity of n- and p-type semiconductors versus temperature. Optical measurements were used to determine the strain shifts and splittings of band extrema [1, 2, 29]. A review of the results at Γ and simple theoretical schemes to estimate the corresponding deformation potentials can be found in [30]. The splittings of the direct excitons of zincblende-type materials under uniaxial strain have been discussed in connection with Figs. 5 and 6.

5.1 Stress-optical functions

The stress (strain)–optical parameters describe the changes in the dielectric function induced by stress (strain) versus frequency. For frequencies below the fundamental gap they have only real components while above that gap they have real and imaginary parts. While considerable information on stress–optical constants *below the gap* has been available for many years, detailed measurements in the absorption region have been performed only in the past few years using ellipsometric techniques.

In a cubic material the stress–optical properties are described by three complex functions of ω_i, p_{11}, p_{12}, and p_{44} (note that they represent a fourth rank tensor which connects the dielectric function with the strain). As an example we display in Fig. 10 the real and imaginary parts of $p_{11}(\omega)$, $p_{12}(\omega)$, $p_{44}(\omega)$ measured ellipsometrically (piezo-ellipsometry) for germanium [4]. These results form a useful data base for optoelectronic applications of the material. The structures labeled E_1 and E_2 correspond to interband critical points and their strength and behavior with increasing stress (i.e., nonlinear in stress phenomena) can be used to determine deformation potentials. It is also possible to calculate the functions $p_{ij}(\omega)$ using electronic band structure techniques of various degrees of sophistication. Empirical pseudopotential methods have been, thus far, most successful. They avoid the so-called "gap problems", ubiquitous in ab initio LDA techniques [4].

5.2 Linear terms in k in the electronic band structure

It is customary to expand electronic band structures around band extrema in power series of the components of $\mathbf{k}$. For most phenomena, only the quadratic terms (related to effective masses) play a role.

Linear terms in $\mathbf{k}$ can sometimes appear [1, 31]. They shift the extrema away from the corresponding high symmetry points. Here we discuss linear terms in $\mathbf{k}$ *induced by stress* at the lowest conduction band minimum and the highest valence band maximum for $\mathbf{k} = 0$. Such terms are of importance in a number of experiments, including cyclotron resonance under stress [32], spin depolarization in luminescence resulting from optical pumping [33] and gyrotropic effects in the dielectric function (including optical rotatory power) [34].

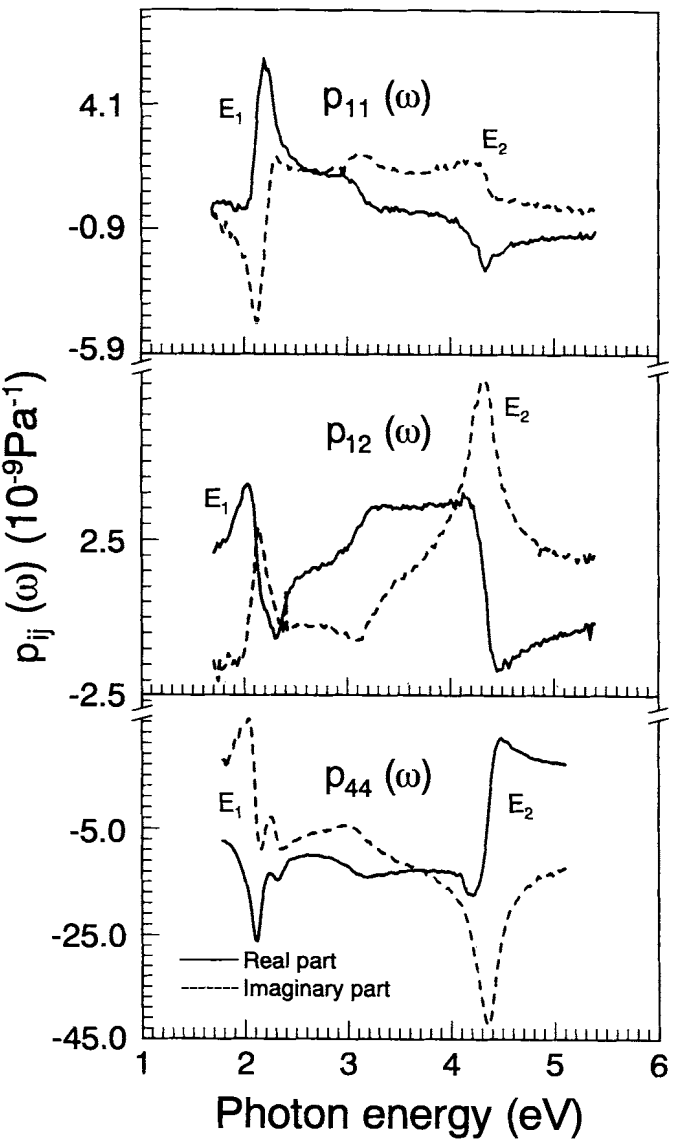

Fig. 10. Real and imaginary parts of the stress-optical constants of germanium measured at room temperature by piezo-ellipsometry. E_1 and E_2 represent well-known interband critical points [4]

The Γ_1 conduction band minimum of zincblende-type materials does not exhibit linear $\mathbf{k}$ terms. Under the action of spin–orbit coupling, however, the spin degeneracy for a given $\mathbf{k} \neq 0$ splits, and cubic (*not linear*) terms in the component $k_{x,y,z}$ of $\mathbf{k}$ are obtained. The equivalent Hamiltonian has the form [1, 31, 35]

$$H^{(3)} = \frac{\gamma}{2} \left(\boldsymbol{\sigma}_x k_x (k_y^2 - k_z^2) + \boldsymbol{\sigma}_y k_y (k_z^2 - k_x^2) + \boldsymbol{\sigma}_z k_z (k_x^2 - k_y^2)\right], \tag{8}$$

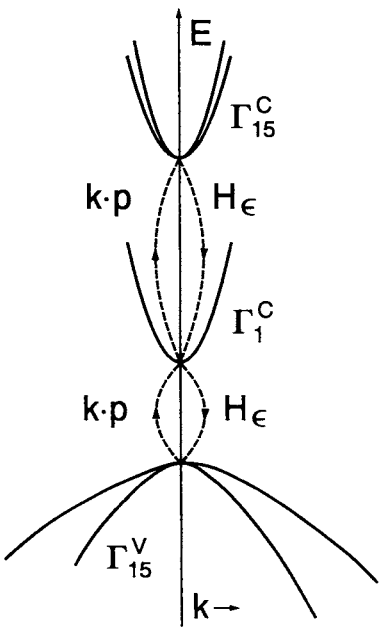

Fig. 11. Schematic diagram of the second order perturbation theory terms which give rise to linear terms in $\mathbf{k}$ at the Γ_1^c conduction band extremum

where $\boldsymbol{\sigma}_{x,y,z}$ represent the Pauli matrices. The xx component of a [100] stress has the same symmetry as k_x^2 and, when replaced into (8) lead to a new equivalent Hamiltonian linear in $(k_y - k_z)$. Likewise, a [111] stress contains terms of symmetries $k_x k_y$, $k_y k_z$, $k_z k_x$ which, when replaced into (8), lead also to linear terms in k.

These terms can be described in $\mathbf{k} \cdot \mathbf{p}$ perturbation theory as shown in Fig. 11 for a [111] stress: the $\mathbf{k} \cdot \mathbf{p}$ Hamiltonian connects the Γ_1^c conduction band with the Γ_{15}^v valence band (also with the Γ_{15}^c conduction band, but this term is less important) thus yielding a factor linear in the components of $\mathbf{k}$. The strain Hamiltonian H_ϵ connects Γ_{15}^v back with Γ_1^c. The corresponding second-order perturbation expression is obtained by dividing the product of the matrix elements of $\mathbf{k} \cdot \mathbf{p}$ and H_ϵ between Γ_{15}^v and Γ_1^c by the $\Gamma_1^c - \Gamma_{15}^v$ energy denominator. The linear terms induced by a Γ_{12}-like [100] stress result from matrix elements which connect Γ_1^c with Γ_{12}-like states. The latter are far away in energy and thus the corresponding linear $\mathbf{k}$ terms are usually negligible. Details of the appropriate matrix elements of H_ϵ and $\mathbf{p}$ are found in [30].

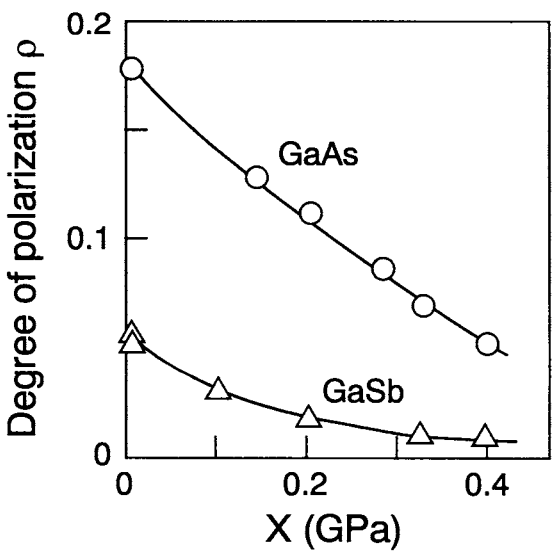

Fig. 12. Polarization of edge luminescence observed in p-type GaAs and GaSb vs. [111] stress. The decrease with increasing stress is due to linear terms in $\mathbf{k}$ generated by the stress [33]

The luminescence produced by a p-type zincblende material upon illumination with circularly polarized light (optical pumping) is also partly circularly polarized [33]. Linear terms in $\mathbf{k}$ in the conduction band structure, induced by a [111] stress, strongly decrease the spin polarization. This effect is illustrated in Fig. 12 for GaAs and GaSb. From the experimentally observed decrease, the coefficient of the stress-induced linear in $\mathbf{k}$ terms can be found. They can also be calculated using the matrix elements of $\mathbf{p}$ and H_ϵ mentioned above [32, 35, 36]. Note that similar linear terms in $\mathbf{k}$ appear also at the Γ_1 conduction bands of superlattices and MQWs fabricated with zincblende-type materials [37]: the lowering of the symmetry is similar to that induced by uniaxial stress.

The valence bands of zincblende-type semiconductors display, at Γ, linear terms in $\mathbf{k}$ even in the absence of stress [1, 36]. These terms, however, are rather small (exception: CuCl, CuBr, CuI) since in the perturbation expressions they have as denominators the energy separation between Γ_{15} and the d-levels of the core ($\gtrsim 10$ eV). Linear terms in $\mathbf{k}$ induced by stress are comparable or larger. They were first considered in connection with cyclotron resonance by holes in InSb [32, 38]. More recently, it has been shown that the $\mathbf{k}$ linear terms induced by a stress along [100] can result in gyrotropy and optical activity (i.e. rotation of the polarization plane for light propagating along either [010] or [001] (the signs of the rotation, however, are opposite for these two propagation directions)). From an analysis of these signs, the sign of the matrix element of H_ϵ between Γ_{15}^c and Γ_{15}^v is found. However, this sign is only meaningful for a given choice of the relative phases in the Γ_{15}^c and Γ_{15}^v wavefunctions [34].

The gyrotropy mentioned above corresponds to *antisymmetric* components of the dielectric tensor linear in $\mathbf{k}$ and in the stress. As mentioned above, there are also stress optical effects (Fig. 10), independent of $\mathbf{k}$, which make the material birefringent. These effects are usually much larger than the gyrotropic terms and thus, by defining a symmetry axis which corresponds to linearly polarized light, they quench the stress-induced optical activity. Below the fundamental gap ($\Gamma_{15}^v \rightarrow \Gamma_1^c$), however, a reversal in the sign of the stress-optical birefringence usually occurs. It is at this so-called isotropic point (frequency) that optical activity can be observed [39].

Acknowledgements I would like to thank E. Anastassakis, P. Etchegoin, B. Koopmans, and P. V. Santos for valuable contributions to the recent work described here. Thanks are also due to S. Birtel for expert help in the composition of the manuscript and to the Fond der Chemischen Industrie for partial support.

References

[1] G. L. BIR and G. E. PIKUS, in: Symmetry and Strain-Induced Effects in Semiconductors, Wiley, New York 1974.
[2] M. CUEVAS and H. FRITZSCHE, Phys. Rev. **137**, A 1847 (1965).
[3] H. VOGELMAN and T. FJELDLY, Rev. sci. Instrum. **45**, 3096 (1974).
F. H. POLLAK and M. CARDONA, Phys. Rev. **172**, 816 (1968).
[4] P. ETCHEGOIN, J. KIRCHER, M. CARDONA, and C. GREIN, Phys. Rev. B **45**, 11721 (1992).
[5] J. PRECHTEL, J. KALUS, E. LÜSCHER, L. PINTSCHOVIUS, and R. GHOSH, phys. stat. sol. (b) **93**, 653 (1979).
J. ESTEL, J. KALUS, and L. PINTSCHOVIUS, phys. stat. sol. (b) **126**, 121 (1984).
[6] B. A. WEINSTEIN and R. ZALLEN, in: Light Scattering in Solids IV, Springer-Verlag, Heidelberg 1984 (p. 463).

[7] P. PAVONE, K. KARCH, O. SCHÜTT, W. WINDL, D. STRAUCH, P. GIANOZZI, and S. BARONI, Phys. Rev. B **48**, 3156 (1993).
A. DEBERNARDI and M. CARDONA, Phys. Rev. B, in press.
[8] V. V. BAPTIZMANSKII, I. I. NOVAK, and YU. F. TITOVETS, Soviet Phys.–Solid State **21**, 1915 (1979).
I. I. NOVAK, V. V. BAPTIZMANSKII, and L. V. ZHOGA, Optika i Spektroskopiya (USSR) **43**, 145 (1977).
[9] G. JONES and D. J. DUNSTAN, Rev. sci. Instrum. **67**, 489 (1996).
[10] S. VES and M. CARDONA, Solid State Commun. **38**, 1109 (1981).
[11] B. ROCKWELL, H. R. CHANDRASEKHAR, M. CHANDRASEKHAR, A.K. RAMDAS, M. KOBAYASHI, and R. L. GUNSHOR, Phys. Rev. B **44**, 11307 (1991).
[12] M. S. BOLEY, R. J. THOMAS, M. CHANDRASEKHAR, H. R. CHANDRASEKHAR, A. K. RAMDAS, M. KOBAYASHI, and R. L. GUNSHAR, J. appl. Phys. **74**, 4136 (1993).
[13] L. J. CUI, V. D. VENKATESWARAN, B. A. WEINSTEIN, and B.T. JONKER, Phys. Rev. B **44**, 10949 (1991).
[14] E. ANASTASSAKIS, Solid State Commun. **84**, 47 (1992).
[15] E. ANASTASSAKIS and M. CARDONA, phys. stat. sol. (b) **104**, 589 (1981).
[16] C. S. G. COUSINS, L. GERWARD, J. STAUN OLSEN, and B. J. SHELDON, J. Phys.: Condensed Matter **1**, 4511 (1989).
[17] C. S. G. COUSINS, L. GERWARD, J. STAUN OLSEN, B. SELSMARK, B. J. SHELDON, and G. E. WEBSTER, Semicond. Sci. Technol. **4**, 333 (1989).
[18] R. M. MARTIN, Phys. Rev. B **1**, 4005 (1970).
[19] P. MOLINÀS-MATA, A. J. SHIELDS, and M. CARDONA, Phys. Rev. B **47**, 1866 (1993).
[20] E. ANASTASSAKIS, A. CANTARERO, and M. CARDONA, Phys. Rev. B **41**, 7529 (1990).
[21] P. RODRÍGUEZ-HERNÁNDEZ, M. GONZÁLEZ DIAZ, and A. MUÑOZ, Phys. Rev. B **51**, 14705 (1995).
[22] M. H. GRIMSDITCH, E. ANASTASSAKIS, and M. CARDONA, Phys. Rev. B **18**, 901 (1978).
[23] O. H. NIELSEN and R. M. MARTIN, Phys. Rev. B **32**, 3792 (1985).
O. H. NIELSEN, Phys. Rev. B **34**, 5808 (1986).
[24] M. METHFESSEL, C. O. RODRIGUEZ, and O. K. ANDERSEN, Phys. Rev. B **40**, 2009 (1989).
[25] S. FAHY, Phys. Rev. B **51**, 12873 (1995).
M. CARDONA and E. ANASTASSAKIS, Phys. Rev. B, in press.
[26] P. WICKBOLDT, E. ANASTASSAKIS, R. SAUER, and M. CARDONA, Phys. Rev. B **35**, 1362 (1987).
[27] J. A. SANJURJO, E. LÓPEZ-CRUZ, P. VOGL, and M. CARDONA, Phys. Rev. B **28**, 4579 (1983).
[28] E. ANASTASSAKIS and M. CARDONA, phys. stat. sol. (b) **129**, 101 (1985).
[29] E. O. KANE, Phys. Rev. **178**, 1368 (1969).
[30] A. BLACHA, H. PRESTING, and M. CARDONA, phys. stat. sol. (b) **126**, 11 (1984).
[31] E. O. KANE, in: Semiconductors and Semimetals, Vol. 1, Academic Press, New York 1966 (p. 75).
[32] H. R. TREBIN, M. CARDONA, R. RANVAUD, and U. RÖSSLER, Proc. Internat. Conf. Physics of Narrow Gap Semiconductors, Warsaw, Sept. 12 to 15, 1977, ed. by J. RAUŁUSKIEWICZ, M. GÓRSKA, and E. KACZMAREK, Polish Sci. Publ., Warsaw 1978 (p. 227).
[33] M. I. DYAKONOV, B. A. MARUSHCHAK, V. I. PEREL, and A. N. TITKOV, Soviet Phys. – J. exper. theor. Phys. **90**, 1123 (1986).
[34] B. KOOPMANS, P. ETCHEGOIN, P. SANTOS, and M. CARDONA, Solid State Commun. **97**, 261 (1996).
[35] M. CARDONA, Proc. HOLSOS'95 Workshop, Sept. 11 to 12, 1995, Frascati (Italy), World Scientific Publ. Co., Singapure, in press.
[36] M. CARDONA, N. E. CHRISTENSEN, and G. FASOL, Phys. Rev. B **38**, 1806 (1988).
[37] P. V. SANTOS, M. WILLATZEN, M. CARDONA, and A. CANTARERO, Phys. Rev. B **51**, 5121 (1995).
[38] R. RANVAUD, R. H. TREBIN, U. RÖSSLER, and F. H. POLLAK, Phys. Rev. B **20**, 701 (1979).
[39] B. KOOPMANS, P. SANTOS, and M. CARDONA, see [35].